JOURNAL OF GEOPHYSICAL RESEARCH, VOL. 113, D03102, doi:10.1029/2007JD008725, 2008



# Detection of migrating diurnal tide in the tropical upper troposphere and lower stratosphere using the Challenging Minisatellite Payload radio occultation data

Zhen Zeng,[1,2,3] William Randel,[4] Sergey Sokolovskiy,[1] Clara Deser,[4] Ying-Hwa Kuo,[1,2] Maura Hagan,[4] Jian Du,[5] and William Ward[5]

Received 29 March 2007; revised 25 September 2007; accepted 24 October 2007; published 2 February 2008.

[1] The atmospheric limb sounding technique making use of radio signals transmitted by the Global Positioning System (GPS) has already proven to be a promising approach for global atmospheric measurements. In this study, we assess for the first time the potential of GPS radio occultation soundings for detecting the migrating diurnal tide. Retrieved temperatures between 10 and 30 km in the tropics from the Challenging Minisatellite Payload (CHAMP) occultation observations during May 2001 to August 2005 are analyzed using space-time spectrum analysis to isolate diurnal waves. Because of incomplete local time (LT) coverage of the monthly CHAMP occultation data in any given year, data from all available years are merged to obtain complete 24-h LT coverage. The effects of aliasing associated with uneven data sampling and measurement noise are estimated using synthetic data. The results show the feasibility of determining tidal structures from the composite CHAMP occultation data, and the vertical, seasonal, and latitudinal structures of the diurnal tide are presented. The estimated diurnal amplitude generally increases with altitude, exhibiting a maximum of order 1 K at 30 km. The estimated phase indicates an upward propagating mode above 14 km with a vertical wavelength about 20 km. The observed diurnal tide at 30 km exhibits a distinct seasonal-latitudinal variation. Comparison of the observed diurnal tide to the simulated tide in the extended Canadian Middle Atmosphere Model (CMAM) and Global-Scale Wave Model Version 2 (GSWM02) indicates that CMAM overestimates the amplitude but reproduces the seasonal-latitudinal variation of the diurnal tide while GSWM02 simulates well the annual mean amplitude but lacks the seasonal-latitudinal variation of the diurnal tide.

**Citation:** Zeng, Z., W. Randel, S. Sokolovskiy, C. Deser, Y.-H. Kuo, M. Hagan, J. Du, and W. Ward (2008), Detection of migrating diurnal tide in the tropical upper troposphere and lower stratosphere using the Challenging Minisatellite Payload radio occultation data, *J. Geophys. Res.*, *113*, D03102, doi:10.1029/2007JD008725.

## 1. Introduction

[2] Atmospheric tides play an important role in the general circulation and the coupling between the lower and the middle and upper atmosphere [*Vial*, 1989; *Kato*, 1989; *Forbes*, 1995; *Hagan*, 2000]. Knowledge of tides is also important for analysis of satellite data sampled at different local solar times, data assimilation [*Swinbank et al.*, 1999] and temperature trend estimation [*Keckhut et al.*, 2001]. Observational and theoretical studies indicate that migrating tides (components that propagate westward with the apparent motion of the Sun) are primarily excited through the zonally symmetric absorption of solar infrared and ultraviolet radiation by tropospheric water vapor and stratospheric ozone, whereas nonmigrating tides (modes which are not Sun-synchronous) are generated by zonally asymmetric thermal forcing (such as planetary boundary layer heat flux, latent heat release in the tropical troposphere) and nonlinear interactions between tides and other propagating waves [*Lieberman*, 1991; *Teitelbaum and Vial*, 1991; *Oberheide et al.*, 2002; *Hagan and Forbes*, 2002, 2003; *Lieberman et al.*, 2004; *Grieger et al.*, 2004].

[3] The characteristics of tides have been established in a number of theoretical works by employing classical tidal theory [*Chapman and Lindzen*, 1970], mechanistic models [*Forbes*, 1982; *Hagan et al.*, 1995; *Hagan*, 2000] and general circulation models [*Tokioka and Yagai*, 1987; *McLandress*, 1997, 2002a]. Ground-based lidar/radar

[1]University Corporation for Atmospheric Research, Boulder, Colorado, USA.
[2]Also at National Center for Atmospheric Research, Boulder, Colorado, USA.
[3]Now at Department of Earth and Ocean Sciences, University of British Columbia, Vancouver, British Columbia, Canada.
[4]National Center for Atmospheric Research, Boulder, Colorado, USA.
[5]Physics Department, University of New Brunswick, Fredericton, New Brunswick, Canada.


0148-0227/08/2007JD008725$09.00

[*Manson et al.*, 2002; *She*, 2004] and satellite observations [*Hays et al.*, 1994; *Burrage et al.*, 1995; *McLandress et al.*, 1996; *Wu et al.*, 1998] provide an assessment of tidal structures in nature and their variability on different scales. Although progress has been made in tidal studies over the past 30 years, because of the limitations of both the space-borne (limited local time coverage and coarse vertical resolution) and ground-based instruments (limited spatial coverage), specification of the global structure and short-term variability of the tides still merits further improvement.

[4] To further investigate the tidal characteristics and their variability, we introduce a relatively new type of data, GPS radio occultation (RO) data, for tidal analysis. These data provide coverage in the upper troposphere and lower stratosphere (UTLS), an altitude range that is lower than that examined in most observational tidal studies. In the GPS RO, radio signals from the GPS satellites, received onboard the LEO (Low Earth's Orbit) satellite, probe the Earth's atmosphere in a limb viewing mode. Propagation of the signals is influenced by the atmospheric refractivity. The fundamental GPS RO observable is the phase delay which is precisely calibrated by ultrastable GPS clock synchronized with the most precise atomic clock on the ground. The phase of the occulted GPS signal is used for deriving atmospheric refractivity, and then temperature, pressure and humidity as functions of altitude [*Kursinski et al.*, 1997]. The proof-of-concept GPS/Meteorology (GPS/MET) experiment and follow-on CHAMP and SAC-C (Satellite de Aplicaciones Cientificas-C) missions have demonstrated high accuracy and vertical resolution and all weather capability of the GPS RO. These and other important characteristics inherent to GPS RO such as self-calibration and mission independence (that allow keeping long-term records without intersatellite calibration) make GPS RO a unique technique for remote sensing of the atmosphere. Another feature of the GPS RO relative simplicity of the instrument (GPS RO receiver), allows launching constellations consisting of large number of GPS RO satellites by increasing density of the observations and providing globally uniform coverage in local time which is important for observation of tides and specification of their short-term variability. The recently launched (15 April 2006) six-satellite COSMIC (Constellation Observing System for Meteorology, Ionosphere and Climate) mission is already in operation and will provide global uniform coverage in local time at the end of 2007 [*Anthes et al.*, 2008]. Following up, there is a plan for launching a 100-satellite GPS RO constellation CICERO (Community Initiative for Continuing Radio Occultation) (http://www.geooptics.com), providing unprecedented global coverage of GPS RO soundings.

[5] In order to assess the feasibility of RO data for tidal study, we first analyze the tropical tides in terms of temperature estimated from the CHAMP RO observations at 10–30 km from May 2001 through August 2005. The German CHAMP mission was launched in July 2000, and its RO soundings have been available since May 2001 [*Wickert et al.*, 2001]. Comparisons of CHAMP RO data with correlative data indicate that CHAMP RO soundings possess the temperature accuracy of 1–2 K in the upper troposphere and lower stratosphere [*Kuo et al.*, 2004, 2005]. Next we compare the observed tidal characteristics with those simulated by the Global-Scale Wave Model Version 2 (GSWM02) [*Hagan and Forbes*, 2002, 2003] and extended Canadian Middle Atmosphere Model (CMAM) [*Beagley et al.*, 2000; *Fomichev et al.*, 2002].

[6] The outline of the paper is as follows: Section 2 provides a detailed description of the temporal and spatial sampling characteristics of the CHAMP RO data and our analysis methodology, with special attention paid to the error estimation. Section 3 briefly describes the two models, CMAM and GSWM02 for comparisons with the CHAMP RO observations. Section 4 presents the results of the tidal analysis, including the vertical structure of the migrating diurnal tide, as well as its latitudinal and seasonal variation. Section 5 summarizes the main results.

## 2. Data and Analysis Method

### 2.1. CHAMP RO Data and Sampling

[7] In this study, we use CHAMP RO temperature profiles between 30°S and 30°N from May 2001 to August 2005 at altitudes 10–30 km. In this altitude range RO temperatures are known to be accurate within 1–2 K. Normally, CHAMP produces 200–250 occultations daily, but after the quality control applied during the inversion, the number of retrieved temperature profiles typically is less.

[8] An important problem arising from using CHAMP RO data for the study of diurnal variations is the local time (LT) coverage. Because of the CHAMP orbit (87° inclination) precession in local time at a rate of ~5.6 min/d, complete 24-h LT coverage would be obtained every ~130 d. However, reception of RO signals from different GPS satellites within approximately ±60° azimuth range allows sampling occultations within approximately ±2000 km band around CHAMP orbit by increasing the coverage and effectively reducing the repeat period to ~108 d at the equator [*Wu et al.*, 2005]. Figure 1a shows the distribution of CHAMP RO data between 5°S and 5°N as a function of day of year and LT. Each color corresponds to observations from a particular year. The local time coverage at other latitudinal bands within 30°S–30°N is similar. It is seen that nearly complete LT coverage can be obtained if the daily data from all years are merged. However, before merging the data, it is important to remove interannual and intra-annual variations (zonally averaged) that may alias into the diurnal cycle. Merging the data from consecutive days further increases the density and uniformity of the data sampling distribution. This will be further described in section 2.2.

### 2.2. Tidal Analysis

[9] All CHAMP RO temperature profiles are interpolated onto a standard vertical grid with 0.2 km resolution from 10 to 30 km altitude. The observations within 30°S–30°N are subdivided into narrower latitude bands 10° in width and overlapping by 5°. Figure 2a shows 90-d running mean RO temperatures zonally averaged between 5°S and 5°N as a function of altitude and time (note the long-term mean for each altitude has been removed for ease of visualization). A strong annual cycle is observed near 18 km with amplitude around 6 K. Above 20 km, the quasi-biennial oscillation (QBO) is prominent, with maximum amplitude around 5 K near 25 km. The QBO signal progresses downward at a rate

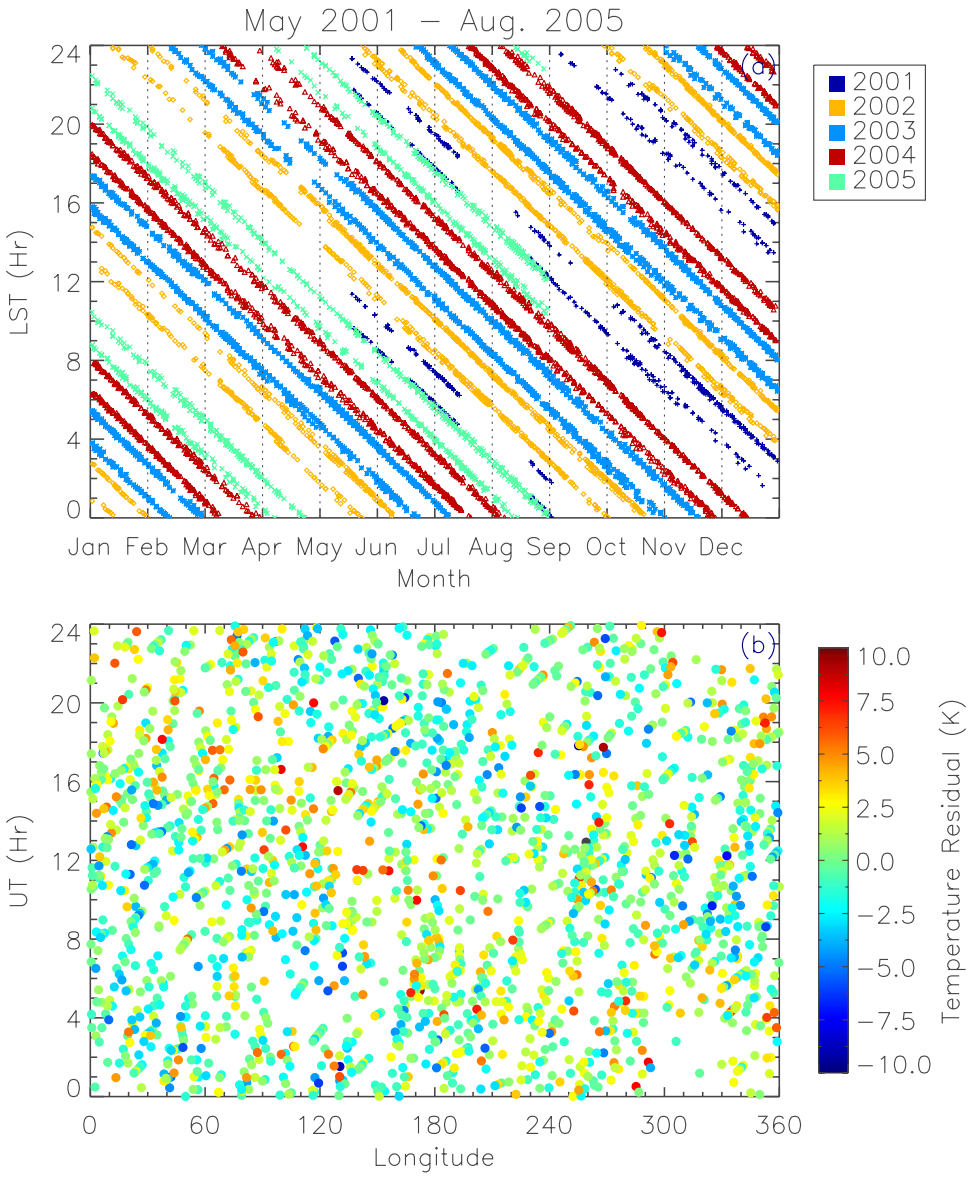


**Figure 1.** (a) Distribution of CHAMP RO soundings between 5°S and 5°N in the coordinates of local solar time (LT) and month. Different colors correspond to different years as indicated. (b) Distribution of CHAMP RO residual temperatures (K) at 30 km for 90-d composite data centered at 15 January between 5°S and 5°N in longitude and UT coordinates.

of approximately 1km/month. Temporal spectral analysis of the temperature residuals shown in Figure 2a confirms the dominance of the annual and QBO signals (Figure 2b). We note that since this study is related to low latitudes (30°S–30°N), in each latitudinal band CHAMP successive samples are separated by about 12 h in LT. Thus the diurnal signal, which is dominant in the LT representation, manifests itself as the high-frequency signal (with CHAMP orbital period about 1.5 h) in the UT representation. This signal is well suppressed by running average and will not alias into the interannual and intra-annual signals significantly. These zonally averaged signals are removed from the daily data from each individual year. Then the daily data from all 4+ years are merged into the composite subsets. Although these subsets cover all LT, their spatial sampling distribution is too sparse and nonuniform for robust spectral analysis. In order to increase the sampling density and uniformity of the spatial coverage, these composite daily subsets from consecutive days are further merged into a composite set, after removal of the daily mean from each subset. Removal of the daily mean is necessary to prevent aliasing of the seasonal signal into the diurnal signal when merging data for consecutive days. Figure 1b shows the distribution of 90-d composite RO data centered at 15 January for 5°S–5°N at 30 km as a function of longitude and universal time (UT). The colors correspond to the temperature residuals from the daily mean. It is evident that the 90-d composite data provide sufficient data density and uniformity for robust estimation of the tidal parameters by space-time spectral analysis and the 90-d composite sets are used in this study. The use of 90-d composite data sets for analysis may result

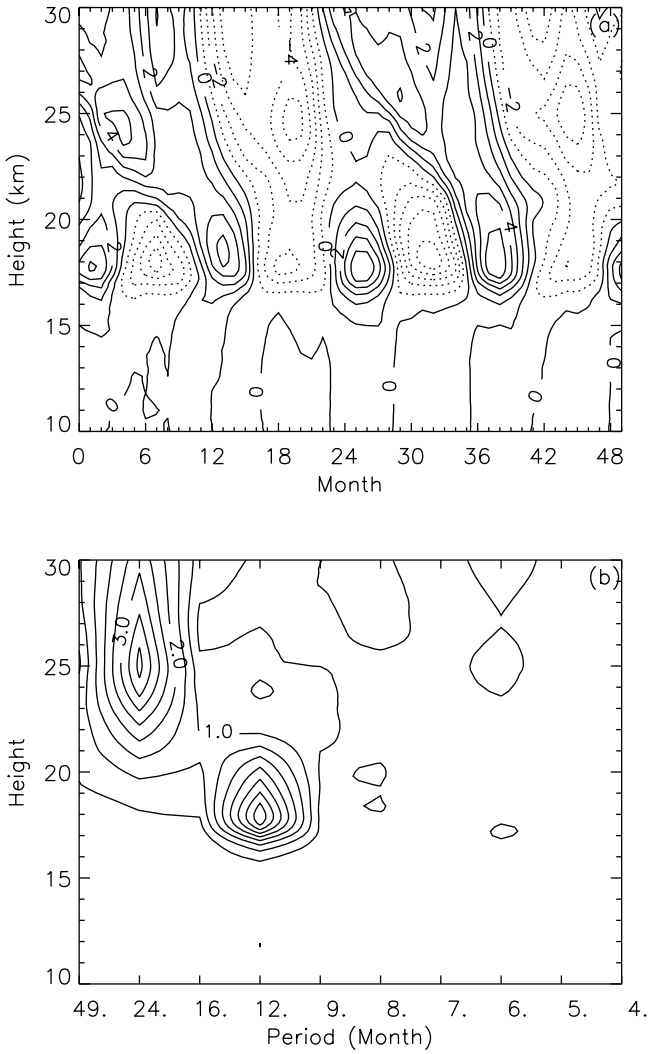


**Figure 2.** (a) Month-altitude cross section of the deviation of 90-d running mean CHAMP RO temperatures from the long-term mean averaged between 5°S and 5°N (contour interval: 1 K). (b) Vertical structure of temporal power spectra of the residual temperature residuals shown in Figure 2a (contour interval: 0.5 K).

in certain smoothing of the seasonal variability of the tidal parameters.

[10] Before applying the space-time spectral analysis, we interpolate the unevenly sampled data (such as that shown in Figure 1b) onto a uniform grid with dimensions of longitude and UT. This is done at each altitude (0.2 km vertical resolution from 10 to 30 km) and latitude (10° bands overlapping by 5° from 30°S to 30°N) separately. The resolution of the uniform grid must allow sufficient spectral bandwidth for higher-order harmonics in order to minimize spectral aliasing that would result in errors in amplitude and phase of the lower-order harmonics. We tested the nearest neighbor interpolation on uniform grids with different resolutions, and found that the results of the spectral analysis become stable, i.e., do not change substantially, in the frequency domain of interest with a grid mesh of at least 64 points × 64 points in the 24 h × 360° longitude domain.

[11] In order to quantitatively estimate the effects of nonuniformity of the data sampling in the UT and longitude coordinates and of the measurement noise on the derived tidal parameters, we use synthetic data based on the function $\sum_{n,s} A_{n,s} \cos(n\Omega t + s\lambda - \phi_{n,s}) + \zeta$, where the first term represents tidal component and second term is the noise; $\Omega$ is the angular frequency of Earth's rotation, $t$ and $\lambda$ are UT and longitude, respectively; $n$ is the frequency in cycles per day and $s$ is zonal wave number (positive for westward propagation); $A_{n,s}$ and $\phi_{n,s}$ are amplitude and phase (time of maximum in UT at the longitude of the Greenwich meridian) of the corresponding tidal component. The measurement noise $\zeta$ is random and normally distributed with standard deviation of 2 K, which is close to the upper estimate of the RO measurement error. We sample the synthetic function at the UTs and longitudes of the CHAMP RO data, then interpolate to the uniform 64×64 mesh, calculate the spectrum and compare the spectral amplitudes and phases with tshe original ones as specified in the function.

[12] Figure 3 shows an example of the spectrum for simulated diurnal tide ($n$ = 1, $s$ = 1) with amplitude $A_{1,1}$ = 1K sampled on the composite distribution centered at January (shown in Figure 1b). Solid and dashed lines show the spectra with and without the measurement noise, respectively. Nonuniformity of the sampling distribution results in aliasing and appearance of high-order harmonics with nonzero amplitudes (this effect is small but still visible as the dashed line is above zero in Figure 3). This results in mean reduction of the tidal amplitudes: by ∼0.5% and ∼1.5% for diurnal and semidiurnal migrating tides, respectively. There is a bias in the phase of about ∼0.35 h for both

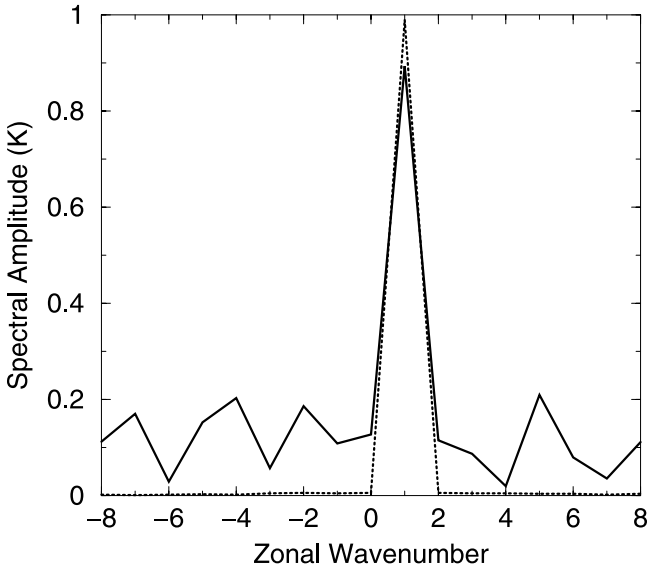


**Figure 3.** An example of the power spectrum of the simulated diurnal tide sampled by a 90-d composite distribution centered at 15 January, with (solid) and without (dashed) measurement noise. See text for details.

diurnal and semidiurnal tides. The standard deviations of the spectral amplitudes induced by 2 K measurement noise are about ~0.1 K for both diurnal and semidiurnal tides. The noise-induced standard deviations of the phases for 1 K tidal amplitude are about 0.2 h and they substantially increase as the tidal amplitude approaches 0.1 K.

### 2.3. An Example of the Tidal Analysis Results

[13] Figure 4 gives an example of the spectral analysis results for the composite data set for the latitude band 5°N–5°S in winter (December, January, February: DJF) (Figures 4a, 4c, and 4e) and summer (June, July, August: JJA) (Figures 4b, 4d, and 4f). Figures 4a and 4b show contour plots of the spectral amplitudes, as functions of zonal wave number and period at 30 km altitude; dashed lines show the locations of migrating tides. In both seasons, the main spectral power is concentrated in the migrating diurnal component with amplitudes ~1 K. In DJF, an additional spectral peak corresponding to the migrating semidiurnal tide is evident. The spectral power in the nonmigrating tidal components is very small in both seasons. The vertical structures of the diurnal and semidiurnal tidal amplitudes are presented in Figures 4c and 4d and Figures 4e and 4f respectively. Dashed lines, as before, show the locations of migrating components. In both seasons, the strongest spectral amplitudes correspond to the migrating diurnal tide, with larger amplitudes in DJF than JJA. The diurnal tidal amplitudes are largest near 30 km (1.0 K versus 0.8 K), and rather weak below ~17 km (the tropopause). The semidiurnal migrating tide (Figures 4e and 4f), in general, is much weaker (especially for JJA) and thus is less clearly distinguishable from the measurement noise (to an even greater extent this is related to other spectral components). In the remainder of this study we will focus only on the migrating diurnal tides (by addressing studies of other components in the tidal spectrum in the future when more dense and uniform data sets are available).

## 3. Models: GSWM02 and CMAM

### 3.1. Global-Scale Wave Model (GSWM) Version 2

[14] The GSWM02, the latest version of the GSWM, simulates monthly mean diurnal and semidiurnal tides excited by climatological monthly mean tidal forcing. It is a two-dimensional, linearized, steady state numerical tidal and planetary-wave model extending from the surface to the thermosphere (~250 km), based on the linearized and extended Navier-Stokes equations for perturbation fields with specified periods and zonal wave numbers upon the zonal mean background atmosphere (http://www.hao.ucar.edu/modeling/gswm/gswm.html). The resolution of GSWM02 is about 4 km in altitude and 3° in latitude. Standard GSWM02 tidal results account for realistic tidal forcing due to the absorption of solar radiation by ozone and water vapor, latent heat release, and the effects of empirical background climatology of zonal mean temperature, neutral density, zonal wind and ozone concentration, as well as wave dissipation. However, the GSWM02 cannot include tidal forcing due to nonlinear wave-mean flow and wave-wave interaction. Next we examine tides in CMAM which includes nonlinear effects.

### 3.2. Extended Canadian Middle Atmosphere Model (CMAM)

[15] The extended CMAM is a 3D spectral general circulation model (GCM) (triangular truncation at total wave number n = 32 (T32) corresponding to a latitudinal-longitudinal resolution of ~6° × 6°) extending from the ground to an altitude of approximately 210 km [see *Beagley et al.*, 2000; *Fomichev et al.*, 2002]. The model contains 70 levels in the vertical with a resolution of approximately 3 km above the tropopause. The model includes heating calculated using comprehensive solar and terrestrial radiative transfer schemes, and parameterizations of latent heat release and convective adjustment. The solar radiation in the model accounts for the absorption in the near infrared by tropospheric water vapor, in the ultraviolet by ozone in the stratosphere and mesosphere, and in the extreme ultraviolet by molecular oxygen in the thermosphere. The terrestrial radiation primarily involves the long-wave radiative transfer by water vapor, ozone and carbon dioxide. Realistic surface topography, planetary boundary layer effects, a full hydrological cycle, and the radiative effects of clouds are included in the model. Water vapor is a prognostic variable so radiative heating/cooling associated with this constituent exhibits considerable variability over a large range of scales. On the other hand, the ozone heating is calculated using ozone climatology and therefore does not exhibit the full range of variability which would develop in the real atmosphere. The model includes the effects of both vertical and horizontal diffusion through physically based parameterizations, as well as the heating by parameterized gravity waves.

[16] The data used for the present study are from the third year of a 4-year model run. The output for this year is considered representative of the model behavior. The atmospheric tides in the model are the results of the combined heating from the various sources listed above. Monthly mean amplitudes for the migrating diurnal tides are computed using model output on 3-h interval as described by *Ward et al.* [2005]. *McLandress* [2002a] demonstrated the capability of this model to reproduce the migrating diurnal tide and its seasonal variation via comparisons with the measurements from the wind imaging interferometer on UARS in the mesosphere and lower thermosphere. In this study we validate the extended CMAM results against the CHAMP RO observations in the UTLS. Both GSWM and CMAM model output are further averaged in the same 10° latitudinal bands and 3-month running windows as the observations.

## 4. Results and Discussion

### 4.1. Vertical Structure of Migrating Diurnal Tide

[17] Figure 5 shows the vertical structure of the monthly temperature amplitudes (Figure 5a) and phases (Figure 5b) of the migrating diurnal tide for the latitude band 5°S–5°N based on 90-d composite data sets centered at the middle of each month (thin black lines). The thick blue lines give the annual mean amplitude and phase. Consistent with Figure 4, the diurnal tidal amplitudes are small (0.1–0.3 K) below 17 km, and reach minimum values near the tropopause (17 km). They increase rapidly with height between 17 km

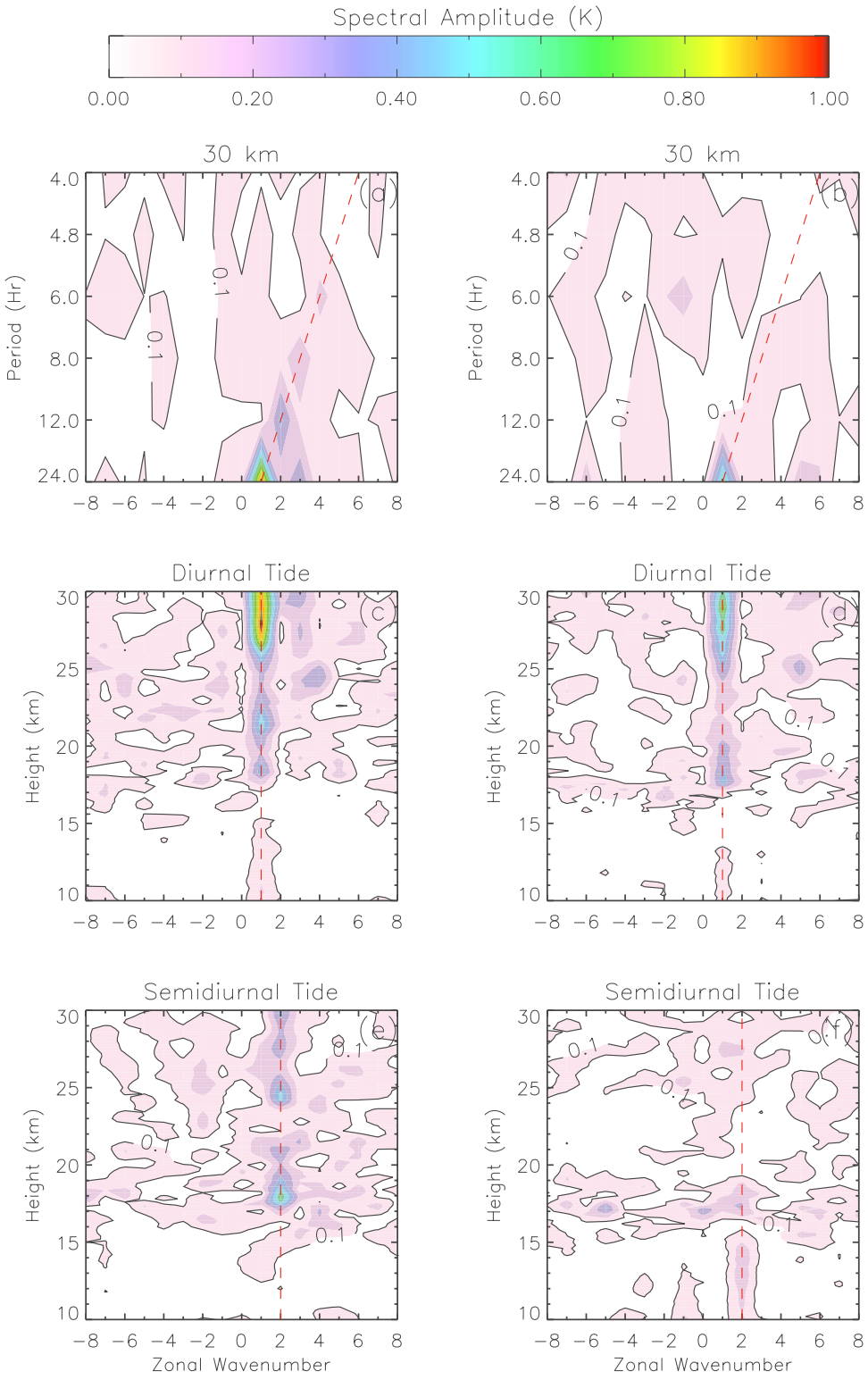


**Figure 4.** Spectral amplitudes of the composite CHAMP RO temperature residuals over 5°N to 5°S (a and b) at 30 km as a function of zonal wave number and period and at 10–30 km as a function of zonal wave number and height for the (c and d) diurnal and (e and f) semidiurnal tides in DJF (Figures 4a, 4c, and 4e) and JJA (Figures 4b, 4d, and 4f). The contour lines indicate the noise level.

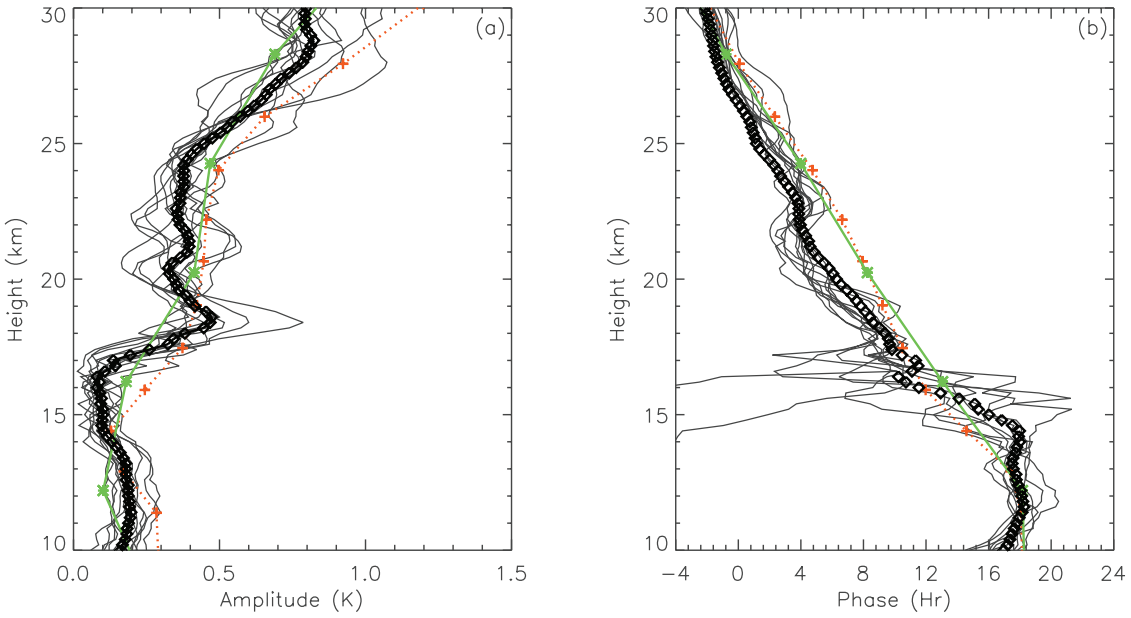


**Figure 5.** Vertical profiles of diurnal temperature (a) amplitudes and (b) phases over 5°S–5°N for composite 90-d subsets centered at the 15th of each month (thin black lines) derived from CHAMP RO observations. The colored curves show the annual mean amplitudes and phases for CHAMP RO observations (blue) and the CMAM (red) and GSWM02 (green) model simulations.

and 18 km, reaching values ~0.4 K, and increase further with altitude above 25 km, reaching maxima ~0.6–1.1 K around 30 km. The annual mean CHAMP RO amplitudes (blue) are in overall good agreement with the CMAM (red) and GSWM02 (green) simulations, although the observations exhibit sharper vertical structures than the model simulations likely because of higher vertical resolution of the observations. CMAM exhibits slightly (10–30%) larger amplitudes than the CHAMP RO data above 25 km. The phases estimated from CHAMP RO data, shown in Figure 5b, decrease with altitude above 14 km, and remain almost constant below 14 km. This indicates an upward propagating diurnal tide above 14 km, and a trapped tide below 14 km in the tropics. It is known that the ozone in the stratosphere is important for forcing the atmospheric tides because of its absorption of solar ultraviolet radiation. However, because of large depth of the ozone layer (around 40–50 km) compared to the vertical wavelength of diurnal tide (see below) the vertical modes forced by the deep ozone heating tend to interfere destructively and do not play an important role in the diurnal tide [*Chapman and Lindzen*, 1970]. On the other hand, heating from the relatively shallow layer of tropospheric water vapor (<10 km) efficiently excites the diurnal tide [*Andrews et al.*, 1987]. The bifurcation of phases near 17 km for some months results from the small amplitudes that are comparable to the noise level. The vertical structure of annual mean phases of the diurnal tide from CHAMP RO observations agrees well with both models, although for the amplitudes there is finer vertical structure in the observations than in the model simulations. The turning point around 22 km in the CHAMP RO data is not simulated by either model. Between 14 km and 22 km, the vertical slope of the phase is smaller in the RO data than in the models. The vertical wavelength (the height interval corresponding to the phase lapse of one full cycle) of the diurnal tide is around 20 km.

[18] The vertical structure of annual mean diurnal amplitude from the CHAMP RO data is in good qualitative agreement with that estimated from four-times-daily radiosonde data from the Tropical Ocean Global Atmosphere/Coupled Ocean Atmosphere Response Experiment [*Seidel et al.*, 2005]. However, the annual mean diurnal phase is almost constant with altitude in the work by *Seidel et al.* [2005], different from the results based on CHAMP RO observations and both model simulations.

### 4.2. Latitudinal and Seasonal Structure of the Migrating Diurnal Tide

[19] In order to give a general view of the latitudinal structure of the migrating diurnal tide, the annual mean amplitudes and phases from CHAMP RO and model simulations are shown in Figure 6. All data sources display maximum amplitudes up to ~1 K at 30 km over the equator, but with CMAM amplitudes being roughly 20% larger than GSWM02 and CHAMP RO. The GSWM02 simulation shows a more symmetric structure of diurnal amplitudes with respect to the equator than CMAM or observations. The annual mean phases from CHAMP RO and both models are in good agreement between 15°S and 15°N, decreasing with altitude. The highly variable phases from CHAMP RO observed near 17 km are related to the small amplitudes. GSWM02 also shows more symmetric phase distribution around the equator than the other data sources.

[20] Figure 7 presents diurnal tidal amplitudes as functions of altitude and latitude of CHAMP RO observations (Figure 7, left), CMAM (Figure 7, middle) and GSWM02 simulations (Figure 7, right) for both solstitial and equinoctial (March, April, May: MAM; September, October, November:

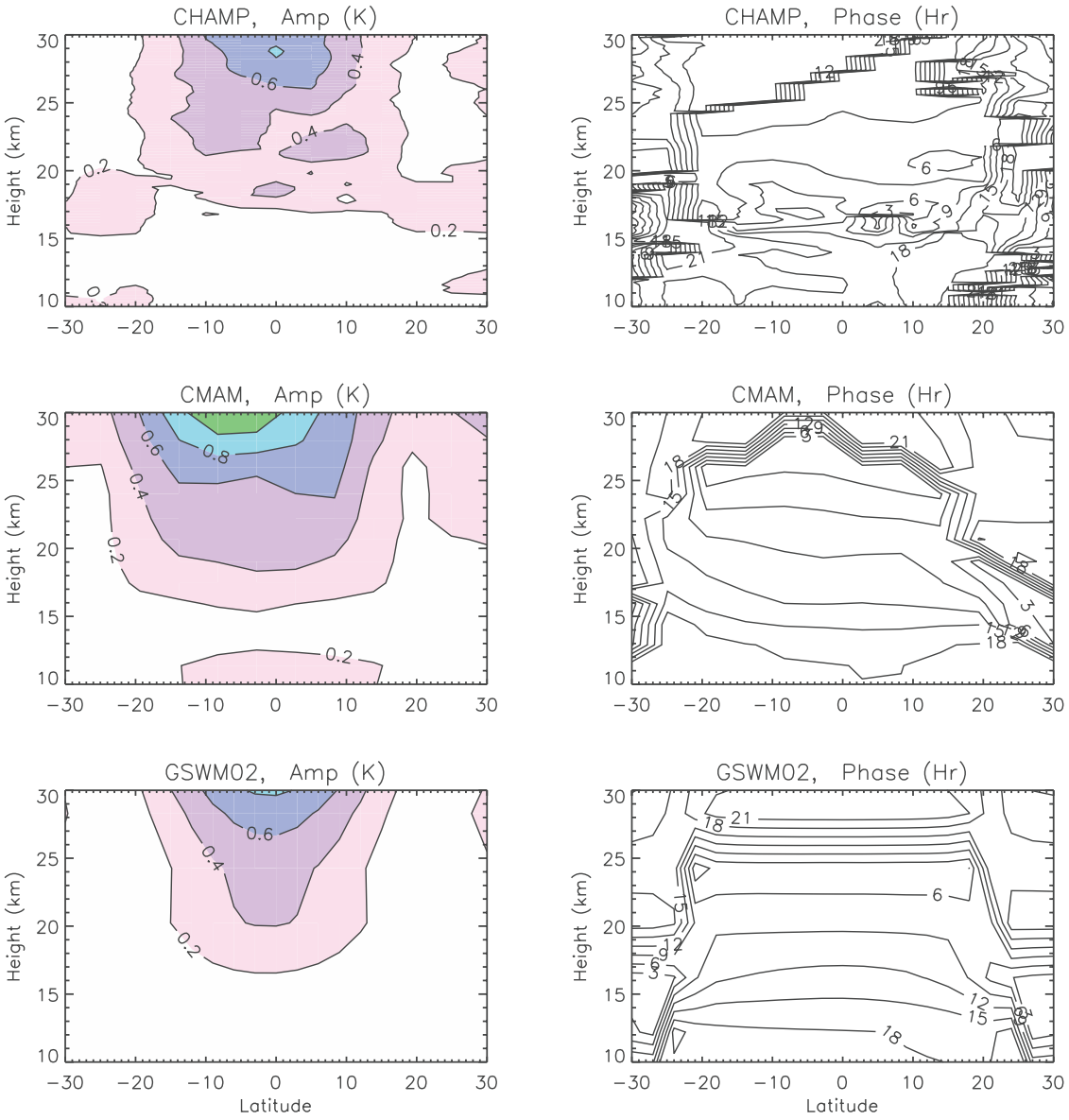


**Figure 6.** Annual mean (left) amplitudes (0.2 K contour interval) and (right) phases (3 h contour interval) of the diurnal tide as a function of height and latitude from (top) CHAMP RO observations and (middle) CMAM and (bottom) GSWM02 model simulations.

SON) seasons. Latitudes and altitudes of maximum amplitude of the diurnal tide are generally in good agreement between CHAMP RO and CMAM. The maxima at 30 km shift from 2–5°N in DJF to 5–10°S in JJA, while lower down the region of large amplitudes shift from 15°S in DJF to 15°N in JJA. During the equinoxes, the maxima at 30 km tend to move to the equator (with some delay for CMAM in SON). This latitudinal-altitudinal variation has been examined using the CMAM [*McLandress*, 1997, 2002b; *MacKenzie*, 2005], and the results showed that it might be caused by the interference of the diurnal latitudinal asymmetric and symmetric modes, which both are excited around the solstice but have slightly different vertical wavelengths. GSWM02 exhibits a rather symmetric amplitude distribution centered at the equator, with peak amplitudes more comparable to those of CHAMP RO and considerably weaker than CMAM. This equator symmetric structure might be related to an overly weak excitation of the asymmetric mode in GSWM02. Stronger tides at equinoxes than those at solstices are clearly evident in GSWM02 but not in observations and CMAM. In addition, the tidal amplitudes below 13 km in GSWM02 are smaller than those from CHAMP RO and CMAM. An additional perspective on seasonal-latitudinal variability of the diurnal tide near 30 km is provided in Figure 8. The latitude of the maximum tidal amplitude shifts with the seasons, occurring at approximately 5°N in November-March and 10°S in May–September in the CHAMP RO data. CMAM exhibits the same seasonal variation, except with a 1–2 month delay. Relatively weak amplitudes are observed during the transi-

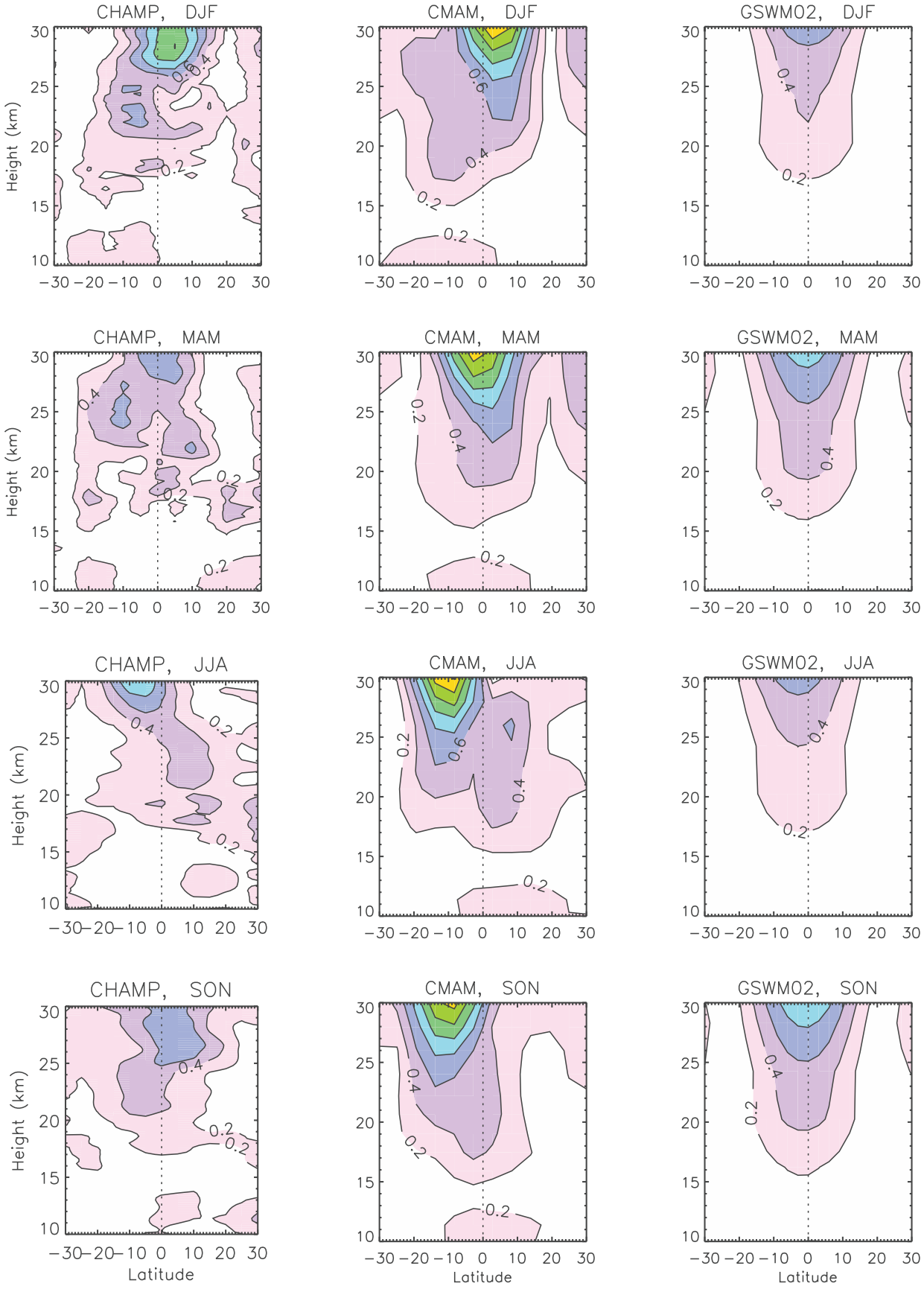


**Figure 7.** Seasonal (DJF, MAM, JJA, and SON) amplitudes of the diurnal tide as a function of height and latitude from the (left) CHAMP RO observations and (middle) CMAM and (right) GSWM02 model simulations. The contour interval is 0.2 K.

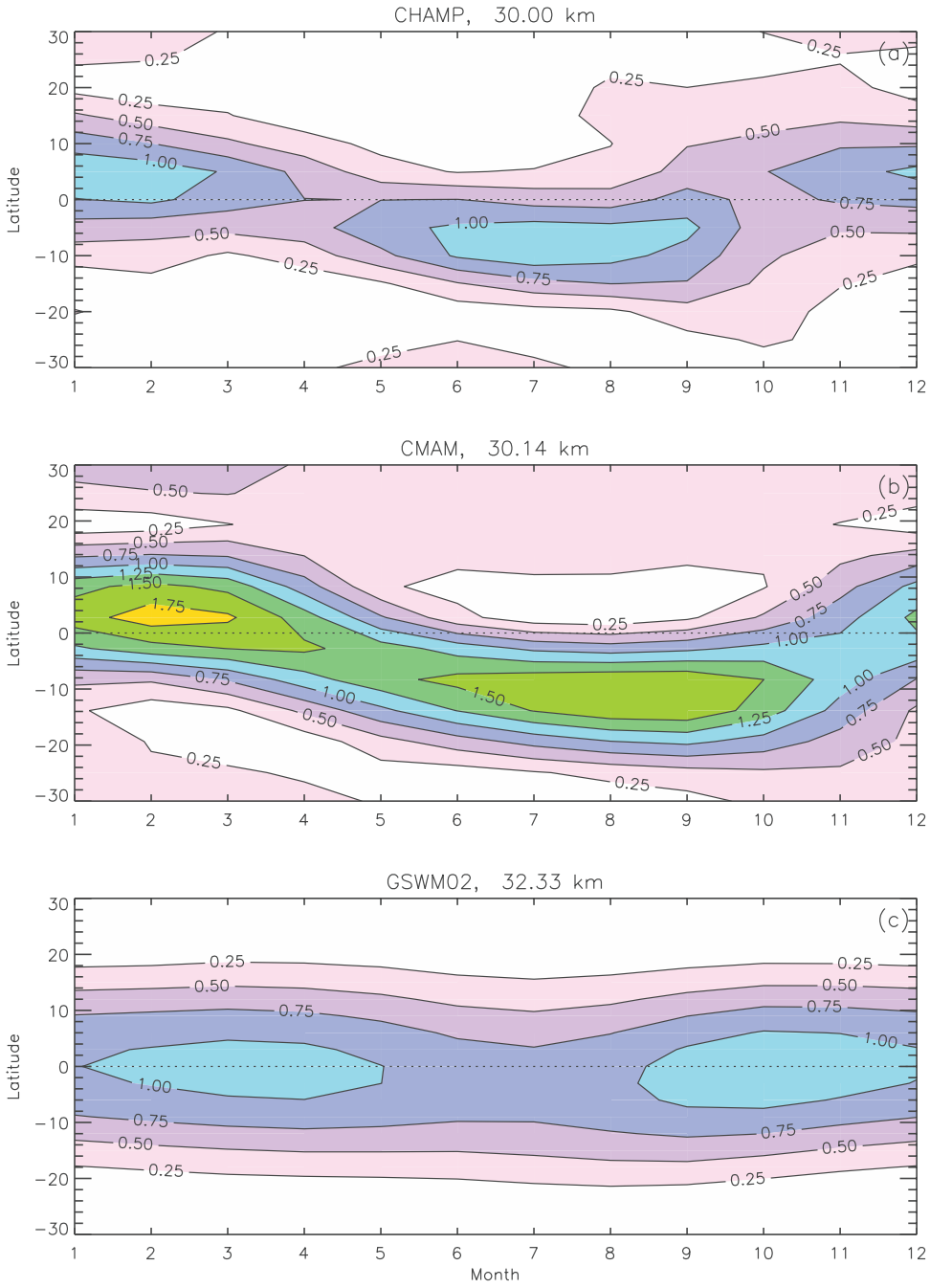


**Figure 8.** Amplitudes of the diurnal tide near 30 km as a function of latitude and month from the (top) CHAMP RO observations and (middle) CMAM and (bottom) GSWM02 model simulations. The contour interval is 0.25 K.

tion months April and October for the CHAMP RO data. The diurnal tide derived from the UARS Microwave Limb Sounder data [*Wu et al.*, 1998] also exhibits similar seasonal-latitudinal structure. In contrast, GSWM02 exhibits maximum amplitudes at the equator throughout the year, with largest values in March and October.

## 5. Summary

[21] In this study, RO data from CHAMP are applied for the first time to estimate the diurnal tidal structures in the tropical UTLS. Although monthly observations suffer from limited LT coverage, the composite data obtained by merging observations for the same day from different years over the CHAMP period of record (51 months), after removing potential aliasing effects from the QBO, allow examination of the tides, and the results of spectral analysis support the validity of this approach.

[22] Mean climatologies of migrating diurnal tide are estimated in terms of vertical, latitudinal and seasonal variations of the tidal parameters. Diurnal tide temperature

amplitudes reach maxima of about 1 K at 30 km near the equator, and show distinct seasonal variations. Diurnal phase indicates an upward propagating diurnal tide above 14 km.

[23] Comparisons of the diurnal migrating tide obtained from CHAMP RO and those from GSWM02 and CMAM models show reasonable agreement in terms of amplitude, phase and seasonality. CMAM tidal simulations are in overall better agreement with the CHAMP RO observations, reproducing many observed features including the seasonal-latitudinal variations of diurnal tide. The GSWM02 shortcomings presented herein are consistent with what *Zhang et al.* [2006] report for migrating tidal temperature diagnostics in the upper stratosphere and mesosphere based upon measurements made by the SABER instrument on the TIMED satellite. That is, the latitude structure of the migrating GSWM02 tide is simpler and more symmetric about the equator than the SABER signatures. The comparison of monthly diurnal tides for CHAMP RO and for SABER measurements at 20–30 km during the 4-year period also shows good agreement in magnitude and phase (X. Zhang, personal communication, 2006).

[24] In this study, only the climatological characteristics of the diurnal tide were resolved because of incomplete sampling of the diurnal cycle in any given year by the CHAMP RO. After full deployment of the six satellites COSMIC (Constellation Observing System for Meteorology, Ionosphere & Climate) mission by evenly separating orbital planes, the tides will be able to be resolved within a single year and hence their interannual variability and small-scale tidal variations may also be assessed.

[25] **Acknowledgments.** This study was funded by a collaborative project between NCAR and UCAR Office of Programs. We thank Jack Fellows and Tim Killeen for their support and encouragement. Special thanks to Kevin Trenberth for his initial suggestions for this study. The National Corporation for Atmospheric Research is supported by National Science Foundation.

## References

Andrews, D. G., J. R. Holton, and C. B. Leovy (1987), *Middle Atmosphere Dynamics*, *Int. Geophys. Ser.*, vol. 40, Elsevier, New York.

Anthes, R. A., et al. (2008), The COSMIC/FORMOSAT-3 mission: Early results, *Bull. Am. Meteorol. Soc*, in press.

Beagley, S. R., C. McLandress, V. Fomichev, and W. E. Ward (2000), The extended Canadian Middle Atmosphere Model, *Geophys. Res. Lett.*, *22*, 2529–2532.

Burrage, M. D., M. E. Hagan, W. R. Skinner, D. L. Wu, and P. B. Hays (1995), Long-term variability in the solar diurnal tide observed by HRDI and simulated by the GSWM, *Geophys. Res. Lett.*, *22*(19), 2641–2644.

Chapman, S., and R. S. Lindzen (1970), *Atmospheric Tides*, D. Reidel, Norwell, Mass.

Fomichev, V. I., W. E. Ward, S. R. Beagley, C. McLandress, J. C. McConnell, N. A. McFarlane, and T. G. Shepherd (2002), Extended Canadian Middle Atmosphere Model: Zonal-mean climatology and physical parameterizations, *J. Geophys. Res.*, *107*(D10), 4087, doi:10.1029/2001JD000479.

Forbes, J. M. (1982), Atmospheric tides: 1. Model description and results for the solar diurnal component, *J. Geophys. Res.*, *87*, 5222–5240.

Forbes, J. M. (1995), Tidal and planetary waves, in *The Upper Mesosphere and Lower Thermosphere: A Review of Experiment and Theory*, *Geophys. Monogr. Ser.*, vol. 87, edited by R. M. Johnson and T. L. Killeen, pp. 67–87, AGU, Washington, D. C.

Grieger, N., G. Schmitz, and U. Achatz (2004), The dependence of nonmigrating diurnal tide in the mesosphere and lower thermosphere on stationary planetary waves, *J. Atmos. Sol. Terr. Phys.*, *66*, 733–754.

Hagan, M. E. (2000), Modeling atmospheric tidal propagation across the stratopause, in *Atmospheric Science Across the Stratopause*, *Geophys. Monogr. Ser.*, vol. 123, edited by D. E. Siskind, S. D. Eckermann, and M. E. Summers, pp. 177–190, AGU, Washington, D. C.

Hagan, M. E., and J. M. Forbes (2002), Migrating and nonmigrating diurnal tides in the middle and upper atmosphere excited by tropospheric latent heat release, *J. Geophys. Res.*, *107*(D24), 4754, doi:10.1029/2001JD001236.

Hagan, M. E., and J. M. Forbes (2003), Migrating and nonmigrating semidiurnal tides in the upper atmosphere excited by tropospheric latent heat release, *J. Geophys. Res.*, *108*(A2), 1062, doi:10.1029/2002JA009466.

Hagan, M. E., J. M. Forbes, and F. Vial (1995), On modeling migrating solar tides, *Geophys. Res. Lett.*, *22*, 893–896.

Hays, P. B., D. L. Wu, and HRDI Science Team (1994), Observations of the diurnal tide from space, *J. Atmos. Sci.*, *51*(20), 3077–3093.

Kato, S. (1989), Non-migrating tides, *J. Atmos. Terr. Phys.*, *51*(8), 673–682.

Keckhut, P., J. D. Wild, M. Gelman, A. J. Miller, and A. Hauchecorne (2001), Investigations on long-term temperature changes in the upper stratosphere using lidar data and NCEP analyses, *J. Geophys. Res.*, *106*(D8), 7937–7944.

Kuo, Y.-H., T.-K. Wee, S. Sokolovskiy, C. Rocken, W. Schreiner, D. Hunt, and R. A. Anthes (2004), Inversion and error estimation of GPS radio occultation data, *J. Meteorol. Soc. Jpn.*, *82*, 507–531.

Kuo, Y.-H., W. S. Schreiner, J. Wang, D. L. Rossiter, and Y. Zhang (2005), Comparison of GPS radio occultation soundings with radiosondes, *Geophys. Res. Lett.*, *32*, L05817, doi:10.1029/2004GL021443.

Kursinski, E. R., G. A. Hajj, K. R. Hardy, J. T. Schofield, and R. P. Linfield (1997), Observing Earth's atmosphere with radio occultation measurements using the Global Positioning System, *J. Geophys. Res.*, *102*(D19), 23,429–23,465.

Lieberman, R. S. (1991), Nonmigrating diurnal tides in the equatorial middle atmosphere, *J. Atmos. Sci.*, *48*(8), 1112–1123.

Lieberman, R. S., J. Oberheide, M. E. Hagan, E. E. Remsberg, and L. L. Gordley (2004), Variability of diurnal tides and planetary waves during November 1978–May 1979, *J. Atmos. Sol. Terr. Phys.*, *66*, 517–528.

MacKenzie, B. D. (2005), A Hough mode decomposition of tidal features found in the extended CMAM, M. S. thesis, Univ. of N. B., Fredericton, N. B., Canada.

Manson, A. H., et al. (2002), Seasonal variations of the semi-diurnal and diurnal tides in the MLT: Multi-year MF radar observations from 2–70°N, modeled tides (GSWM, CMAM), *Ann. Geophys.*, *20*, 661–677.

McLandress, C. (1997), Seasonal variability of the diurnal tide: Results from the Canadian Middle atmospheric general circulation model, *J. Geophys. Res.*, *102*, 29,747–29,764.

McLandress, C. (2002a), Seasonal variation of the propagating diurnal tide in the mesosphere and lower thermosphere. Part I: The role of gravity waves and planetary waves, *J. Atmos. Sci.*, *59*(5), 893–906.

McLandress, C. (2002b), The seasonal variation of the propagating diurnal tide in the mesosphere and lower thermosphere. Part II: The role of tidal heating and zonal mean winds, *J. Atmos. Sci.*, *59*(5), 907–922.

McLandress, C., G. G. Shepherd, and B. H. Solheim (1996), Satellite observations of thermospheric tides: Results from the Wind Imaging Interferometer on UARS, *J. Geophys. Res.*, *101*(D2), 4093–4114.

Oberheide, J., M. E. Hagan, R. G. Roble, and D. Offermann (2002), Sources of nonmigrating tides in the tropical middle atmosphere, *J. Geophys. Res.*, *107*(D21), 4567, doi:10.1029/2002JD002220.

Seidel, D. J., M. Free, and J.-H. Wang (2005), Diurnal cycle of upper-air temperature estimated from radiosondes, *J. Geophys. Res.*, *110*, D09102, doi:10.1029/2004JD005526.

She, C.-Y. (2004), Initial full-diurnal-cycle mesopause region lidar observations: diurnal-means and tidal perturbations of temperature and winds over Fort Collins, CO (41°N, 105°W), *J. Atmos. Sol. Terr. Phys.*, *66*, 663–674.

Swinbank, R., R. L. Orris, and D. L. Wu (1999), Stratospheric tides and data assimilation, *J. Geophys. Res.*, *104*, 16,929–16,947.

Teitelbaum, H., and F. Vial (1991), On tidal variability by nonlinear interaction with planetary wave, *J. Geophys. Res.*, *96*, 14,169–14,178.

Tokioka, T., and I. Yagi (1987), Atmospheric tides appearing in a global atmospheric general circulation model, *J. Meteorol. Soc. Jpn.*, *65*, 423–437.

Vial, F. (1989), Tides in the middle atmosphere, *J. Atmos. Terr. Phys.*, *51*(1), 3–17.

Ward, W. E., V. I. Fomichev, and S. Beagley (2005), Nonmigrating tides in equinox temperature fields from the Extended Canadian Middle Atmosphere Model (CMAM), *Geophys. Res. Lett.*, *32*, L03803, doi:10.1029/2004GL021466.

Wickert, J., et al. (2001), Atmosphere sounding by GPS radio occultation: First results from CHAMP, *Geophys. Res. Lett.*, *28*, 3263–3266.

Wu, D. L., C. McLandress, W. G. Read, J. W. Waters, and L. Froidevaux (1998), Equatorial diurnal variations observed in UARS Microwave

Limb Sounder temperature during 1991–1994 and simulated by the Canadian Middle Atmosphere Model, *J. Geophys. Res.*, *103*(D8), 8909–8917.

Wu, D. L., C. O. Ao, G. A. Hajj, M. T. Juarez, and A. J. Mannucci (2005), Sporadic E morphology from GPS-CHAMP radio occultation, *J. Geophys. Res.*, *110*, A01306, doi:10.1029/2004JA010701.

Zhang, X., J. M. Forbes, M. E. Hagan, J. M. Russell III, S. E. Palo, and M. Mlynczak (2006), Monthly tidal temperatures 20–120 km from TIMED/SABER, *J. Geophys. Res.*, *111*, A10S08, doi:10.1029/2005JA011504.

C. Deser, M. Hagan, and W. Randel, National Center for Atmospheric Research, Boulder, CO 80305, USA.

J. Du and W. Ward, Physics Department, University of New Brunswick, Fredericton, NB, Canada E3B 5A3.

Y.-H. Kuo and S. Sokolovskiy, University Corporation for Atmospheric Research, Boulder, CO 80307, USA.

Z. Zeng, Department of Earth and Ocean Sciences, University of British Columbia, Vancouver, BC, Canada V6T 1Z4. (zzeng@eos.ubc.ca)